ISSN 0021-3640, JETP Letters, 2022, Vol. 116, No. 4, pp. 240–245. © Pleiades Publishing, Inc., 2022.
Russian Text © The Author(s), 2022, published in Pis'ma v Zhurnal Eksperimental'noi i Teoreticheskoi Fiziki, 2022, Vol. 116, No. 4, pp. 242–248.

CONDENSED MATTER

Activation Energy and Mechanisms for Skyrmion Collapse in Synthetic Antiferromagnets

K. V. Voronin[a], I. S. Lobanov[a], and V. M. Uzdin[a, *]

[a] *Faculty of Physics, ITMO University, St. Petersburg, 197101 Russia*

**e-mail: v_uzdin@mail.ru*

Received June 24, 2022; revised July 3, 2022; accepted July 4, 2022

The mechanisms of the collapse of skyrmion structures in synthetic antiferromagnets and the activation energy of such processes are studied within the transition state theory based on the analysis of the multidimensional energy surface of the system and the construction of minimum energy paths between the corresponding states. Synthetic antiferromagnets consist of two thin ferromagnetic films separated by a nonmagnetic metal spacer, the conduction electrons of which provide antiferromagnetic interlayer exchange interaction. A discrete Heisenberg-type model is used, which includes symmetric and antisymmetric exchange in each layer, interaction with the applied magnetic field, and the aforementioned interlayer exchange interaction. The experimentally observed magnetic structures are reproduced. It is shown that the most probable mechanism for the collapse of skyrmion pairs involves an asymmetric state with a skyrmion in one layer. The activation energy for such a process is calculated. It is 16% lower than the numerical estimates based on the micromagnetic ansatz, but is a factor of 1.4 higher than that corresponding to the annihilation of a skyrmion of the same size in one layer.

DOI: 10.1134/S0021364022601361

1. INTRODUCTION

Magnetic skyrmions are localized magnetic states, the stability of which with respect to random external fields is attributed to the existence of a topological charge, which remains unchanged under the continuous variation of the magnetization [1]. These systems can be used as information bits for a new generation of ultradense and fast magnetic memory [2, 3]. Because of the nonlinear dynamic response of skyrmions to applied fields, they can be considered as possible elements of neuromorphic devices and artificial neural networks [4]. However, the use of ferromagnetic (FM) materials as carriers of skyrmion states encounters a number of difficulties that hinder their actual applications. Among them are the relatively large size of skyrmions stable at room temperature [5], which reduces the density of information storage, the presence of a Hall angle at the motion under the effect of a spin-polarized current [6], and demagnetization fields that complicate the control of the dynamics of skyrmion states, as well as the architecture and design of magnetic racetrack memory.

These difficulties can be avoided to a large extent by using antiferromagnetic [7] and ferrimagnetic materials [8, 9], in which topological chiral structures are localized. Skyrmions up to 10 nm in size, stable at room temperature, were found experimentally in ferrimagnetic Pt/GdFeCo [10] and Pt/GdCo [11] films. Near the compensation point, these systems behave like skyrmions in an antiferromagnetic (AFM) medium. The stability and lifetimes of FM and AFM skyrmion structures were studied within the transition state theory in [12]. The size of a skyrmion increases with the applied magnetic field in AFM materials, while in FM materials, it decreases if the field is directed opposite to the magnetization at the center of the skyrmion. Nevertheless, a relation can be established between these states, in which their energy surfaces and activation barriers for the collapse coincide. This allows one to estimate the lifetimes of AFM skyrmions without additional calculations if the corresponding values for the FM analogs are known.

It is difficult to detect skyrmions in AFM materials since the magnetic structure in the center of a skyrmion and outside it is nearly the same. From this viewpoint, the concept of synthetic antiferromagnets (SAFMs), in which chiral skyrmions and domain walls can be formed [13–15], is quite topical. In these systems, chiral topological configurations, in particular, skyrmions, arise in ferromagnetic films with AFM exchange acting across a thin nonmagnetic spacer. Skyrmions in films form bound states, and the demagnetizing fields generated by each of them largely compensate each other, as in the case of an AFM medium. Therefore, even for magnetic films with a thickness of several nanometers, the magnetostatic interaction, which leads to an increase in the size of topological structures [16], can be neglected. As a result, it is pos-

sible to obtain stable skyrmion pairs with a characteristic size up to 10 nm at room temperature. However, an accurate calculation of the stability of such structures with respect to thermal fluctuations has not yet been carried out. The most consistent method for quantifying the stability of magnetic states, including the activation energy of transfer processes between them, is based on the theory of the transition state for magnetic degrees of freedom [17, 18]. In this work, we perform such calculations for skyrmions in SAFMs and analyze the most probable mechanism of their decay.

2. DISCRETE MODEL AND MAGNETIC CONFIGURATIONS

To describe the properties of bound skyrmion states in SAFMs, we study the structure in which these states were observed in experiments [14]. A SAFM consists of two magnetic layers separated by a nonmagnetic metal layer. The effective exchange interaction between magnetic layers, described by the Ruderman–Kittel–Kasuya–Yosida (RKKY) mechanism, oscillates with the thickness of the nonmagnetic spacer. This thickness is chosen so that the interlayer interaction is of the AFM type. The magnetic layers are Co films with a heavy metal (Pt) at the interface, which induces the Dzyaloshinskii–Moriya antisymmetric exchange in the magnetic subsystem. At the same time, the presence of the Pt/Co interface leads to the easy axis anisotropy with the axis orthogonal to the film plane. However, this anisotropy is compensated by the easy plane anisotropy arising owing to the magnetostatic interaction, which depends on the thickness of the magnetic layers, at $d = 1.47$ nm.

Such a system can be described by a lattice model based on the Heisenberg-type Hamiltonian, which includes, along with the intralayer exchange interaction and Dzyaloshinskii–Moriya exchange, the RKKY interlayer interaction:

$$E = -\sum_{n=1,2}\sum_{\langle i,j\rangle}(J\mathbf{S}_i^n\cdot\mathbf{S}_j^n + \mathbf{D}_{ij}\cdot[\mathbf{S}_i^n\times\mathbf{S}_j^n]) - \sum_i J_{12}\mathbf{S}_i^1\cdot\mathbf{S}_i^2. \quad (1)$$

Here, $\mathbf{S}_i^n$ is a three-dimensional unit vector directed along the magnetic moment at the ith site in the nth SAFM layer, the summation is performed over nearest neighbor i, j pairs, the parameters of the intralayer Heisenberg exchange J and the Dzyaloshinskii–Moriya vector $\mathbf{D}_{ij}$ ($|\mathbf{D}_{ij}| = D$) are nonzero only for moments at neighboring sites and are the same within both layers, and the interlayer exchange interaction parameter J_{12} is related to the spin polarization of conduction electrons induced by magnetic layers in the nonmagnetic interlayer. In the simplest approximation, this interaction has the same local form as the Heisenberg exchange. It is possible to consider a more general model, in which the magnetic moment interacts not with the moment located at the nearest site in the second layer, but with the average magnetic moment in a certain region around this site. However, the qualitative picture of magnetic configurations in this case remains the same.

The parameters of the discrete model were chosen to correspond to the values measured in the experiment and the data used in micromagnetic simulation [14, 19]. The calculations presented below are performed for plane square and triangular lattices corresponding to the same continuous model under the assumption that the magnetic state is uniform over the thickness of each magnetic layer. The magnetic configurations and their energy characteristics are nearly the same for both lattices. Therefore, only the results obtained for the square lattice will be presented. In the absence of anisotropy, the ground state of the magnetic layers corresponds to a spiral structure determined by the ratio of the parameters of the exchange and Dzyaloshinskii–Moriya interactions. The presence of the AFM interlayer interaction leads to an antiparallel correlation of the directions of magnetic moments in the spin spirals of different layers. The corresponding magnetic configurations obtained in the calculation performed with the parameters $J = 183$ meV, $D = 6.9$ meV, and $J_{12} = 3.24$ meV on a 1000×1000 grid with the step $a = 1.5$ nm and periodic boundary conditions are shown in Figs. 1a and 1b. The period of the spiral structure in Fig. 1a corresponds to the theoretical estimate $L = 2\pi aJ/D$.

To obtain spatially localized pairs of bound skyrmion states in the SAFM, magnetic layers $[\mathrm{Pt}(0.45\ \mathrm{nm})/\mathrm{Co}(0.6\ \mathrm{nm})]_4$ with strong uniaxial anisotropy perpendicular to the film plane were additionally introduced into the system. These layers induce an effective magnetic field $\mathbf{H}_b$ via the Pt spacer in the nearest SAFM magnetic layer with $n = 1$. We refer to this layer as lower according to the geometry of the samples used in experiments [14]. The mechanism of formation of this field, as well as of the J_{12} exchange, is related to the RKKY interaction involving conduction electrons of the nonmagnetic spacer. However, the thickness of the nonmagnetic layer here is chosen such that the interlayer exchange is ferromagnetic. Thus, the proximity effect related to the additional magnetic layer is reduced to supplementing the energy (1) by a term of the same type as the applied magnetic field, which acts only on the lower magnetic layer. Together with the interaction with the applied field $\mathbf{H}_{\mathrm{ext}}$, the total energy is now written as

$$E_{\mathrm{SAF}} = E - \sum_i \mu\mu_0[(\mathbf{H}_b + \mathbf{H}_{\mathrm{ext}})\cdot\mathbf{S}_i^1 + \mathbf{H}_{\mathrm{ext}}\cdot\mathbf{S}_i^2], \quad (2)$$

where μ is the magnetic moment of the cell of the grid.

In Figs. 1c and 1d, we show the skyrmion states arising in the (c) lower and (d) upper layers at $\mu_0 H_b = 50$ mT and $\mu = 430\mu_B$. The remaining param-

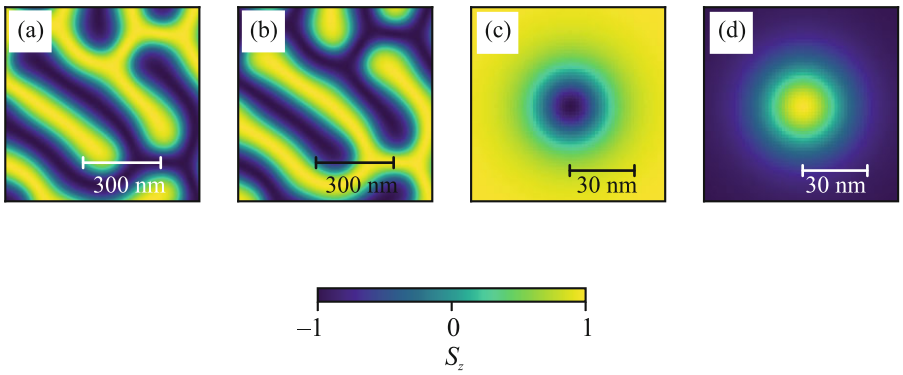

Fig. 1. (Color online) Color maps of the z projection of the vector **S** in the synthetic antiferromagnet for (a, b) magnetic spirals in the (a) lower and (b) upper layers in the presence of Dzyaloshinskii–Moriya interaction and interlayer antiferromagnetic exchange and (c, d) skyrmions in the (c) lower and (d) upper layers at the antiferromagnetic interlayer exchange and in the field $H_b = 50$ mT induced in the lower layer by additional magnetic layers owing to the Ruderman–Kittel–Kasuya–Yosida interaction.

eters here are the same as for the system shown in Figs. 1a and 1b.

With a change in the interlayer exchange interaction J_{12}, the structure of the skyrmion states in both SAFM magnetic layers is modified, but to a larger extent in the upper one. The value and sign of J_{12} depends on the thickness of the nonmagnetic spacer. The thickness can be changed even within the same sample by using the wedge nonmagnetic layer [20]. In this case, one can expect the formation of various magnetic configurations upon displacement in the plane of the sample and the transformation of magnetic structures during their motion under the effect of a spin-polarized current. When starting from the state shown in Figs. 1c and 1d and decreasing the AFM coupling value, the skyrmion size in the upper layer increases. At the interaction close to zero, a spiral magnetic structure is restored in this layer, as seen in Fig. 1b. A change in the sign of J_{12} leads to the formation of a bound skyrmion state in the upper layer with moments codirectional with those in the lower layer. For large values of $|J_{12}|$, the sizes of skyrmions in both layers become almost the same.

Let us now consider the evolution of the magnetic structure with a change in the applied field $\mathbf{H}_{ext}$. In a single-layer system, an increase in the field leads to the transition from the spiral structure to the skyrmion states and then to a decrease in the stability and radius of the skyrmion up to its vanishing and the transition of the system to the FM state. In the SAFM at $J_{12} < 0$, an increase in the magnetic field reduces the size of the skyrmion in the lower layer and increases it in the upper one. The RKKY interaction of the magnetic moments of the upper layer with the lower one competes with the applied field, and the dependence of the skyrmion size in the lower layer on the applied field is not obvious a priori. In Fig. 2, we show the dependence of the skyrmion radii in the lower and upper layers on the magnetic field applied in the direction perpendicular to the plane of the system at a fixed value of $\mu_0 H_b = 50$ mT.

With an increase in the magnetic field, the radius of bound skyrmions increases both in the lower and upper layers, but in the upper layer, this increase is faster. When the direction of the applied field is changed, the size of the skyrmions first decreases. If $\mathbf{H}_b + \mathbf{H}_{ext} = -\mathbf{H}_{ext}$, the skyrmion radius is the same in both layers.

At $\mathbf{H}_b = -\mathbf{H}_{ext}$, the magnetic configuration is equivalent to the SAFM state at zero magnetic field, in which the upper magnetic layer is replaced by the lower one, and vice versa. A further increase in the skyrmion radii at $H_{ext} < -H_b$ occurs, as in the case of $H_{ext} > 0$, if the layers are interchanged. Note that an increase in the equilibrium radius of skyrmions in AFM films with an increase in the applied magnetic field was obtained in [12].

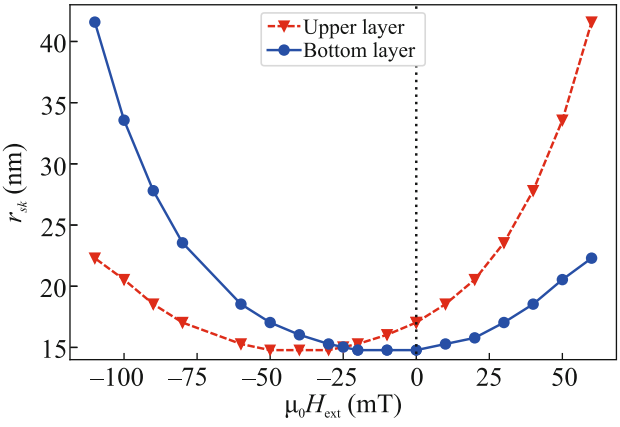

Fig. 2. (Color online) Radii r_{sk} of bound skyrmions in the lower and upper magnetic layers of the synthetic antiferromagnet versus the applied magnetic field at $\mu_0 H_b = 50$ mT.

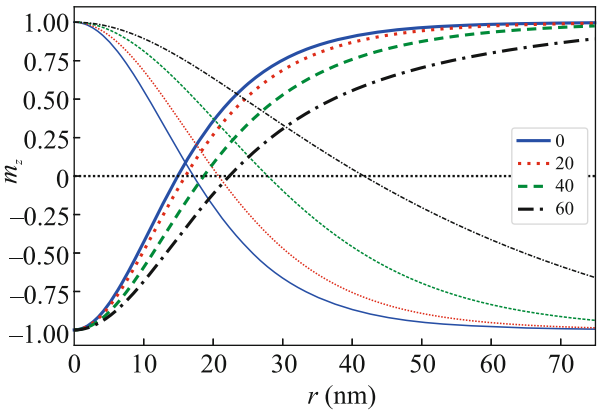

Fig. 3. (Color online) Magnetic profiles of skyrmions $m_z(r)$ in the (thick lines) lower and (thin lines) upper layers of the synthetic antiferromagnet at different values of the applied field and $\mu_0 H_b = 50$ mT.

A change in H_b is equivalent to a shift of the plots shown in Figs. 2 along the horizontal axis, so that the radii of the skyrmions coincide at $H_{ext} = -H_b/2$.

In Fig. 3, we show the magnetization profiles of skyrmions in the lower and upper layers at $\mu_0 H_b =$ 50 mT and different values of H_{ext}. The plots similar to those shown in Fig. 3 were obtained in [14] using the micromagnetic simulation. Some differences, such as the coincidence of the skyrmion radii in both layers at $\mu_0 H_{ext} \approx 20$ mT, may be due to the dipole interaction taken into account in the micromagnetic software, but not included in the expression for energy (2).

3. MINIMUM ENERGY PATHS AND THE SKYRMION STABILITY IN THE SAFM

A quantitative characteristic of the stability of magnetic states with respect to thermal fluctuations and random perturbations can be their average lifetime. An expression obtained for this quantity in the harmonic approximation of the transition state theory corresponds to the Arrhenius law [18, 21]

$$\tau = \tau_0 \exp\left(\frac{\Delta E}{k_B T}\right), \qquad (3)$$

where ΔE is the activation energy for the magnetic state collapse. To calculate this quantity, the energy surface of the system is studied as a functional of all variables that uniquely determine the magnetic configuration. The local minima on the energy surface correspond to the ground and metastable states, whereas the minimum energy path (MEP) between them determines the most probable scenario of the magnetic transition [22, 23]. The maximum along the path is a first-order saddle point, and the activation barrier is calculated as the difference between the energies at the saddle point and the initial state: $\Delta E = E_{sp} - E_{min}$. The pre-exponential factor τ_0 in (3) depends on the entropy of the system in the initial state and at the saddle point, as well as on the dynamics that determine the rate of departure from the saddle point in the direction toward the final state [18, 24].

The calculations of the MEP for the collapse of a skyrmion pair in the SAFM were performed on a square lattice of 500 × 500 sites with periodic boundary conditions. If the directions of spins are specified by two angles in the polar coordinate system, the dimension of the energy surface of the system is 500000. However, it is more convenient to use Cartesian coordinates. In this case, the dimension of the surface increases, and the conservation law for the magnetic moments is taken into account by introducing the Lagrange multipliers [18]. The large dimension of the energy surface makes the calculation of the saddle point a difficult computational problem. Here, it is possible to calculate the MEP near the saddle point using the truncated MEP method [25].

In Fig. 4, we show the MEP between the state with two bound skyrmions in the magnetic layers of the SAFM and the uniform state with FM ordering in each layer. The parameters correspond to those of the continuous model and experimental data [14]: $J =$ 183.75 meV, $D/J = 6.3 \times 10^{-3}$, $J_{12}/J = 5 \times 10^{-4}$, $\mu = 12\mu_B$, and $\mu_0 H_b = 50$ mT in the absence of the applied magnetic field. In the right panels, magnetic configurations are shown at the points marked along the path in the left panel. The path goes via an intermediate minimum corresponding to the equilibrium state with one skyrmion in the upper layer. However, the barrier separating it from homogeneous FM ordering is as low as $0.03J$, and the lifetime of such a skyrmion is many orders of magnitude smaller than that of a coupled pair of skyrmions in the SAFM.

In the initial equilibrium state, the sizes of skyrmions in both layers are nearly the same. In the part of the MEP up to the first saddle point, the radii of the skyrmion states decrease, but in the lower layer the decrease is more pronounced than in the upper one. The activation barrier that must be overcome for the decay of a skyrmion pair is $\Delta E = 4.9J$. Then, the skyrmion collapses in the lower layer with a reversal of moments at the center of the skyrmion, and a further transition to a homogeneous state occurs. In the upper layer, the skyrmion continues to contract even after the first saddle point, passing into a locally stable state. In this case, the energy of the system remains nearly unchanged. In this part of the path, the main contribution to the energy measured from the homogeneous FM state is due to the exchange interaction. For topological solitons in two-dimensional isotropic ferromagnets, the scaling transformation corresponding to the breathing mode does not change the energy of the system [1]. Therefore, the energy along the path is practically constant and close to the minimum energy

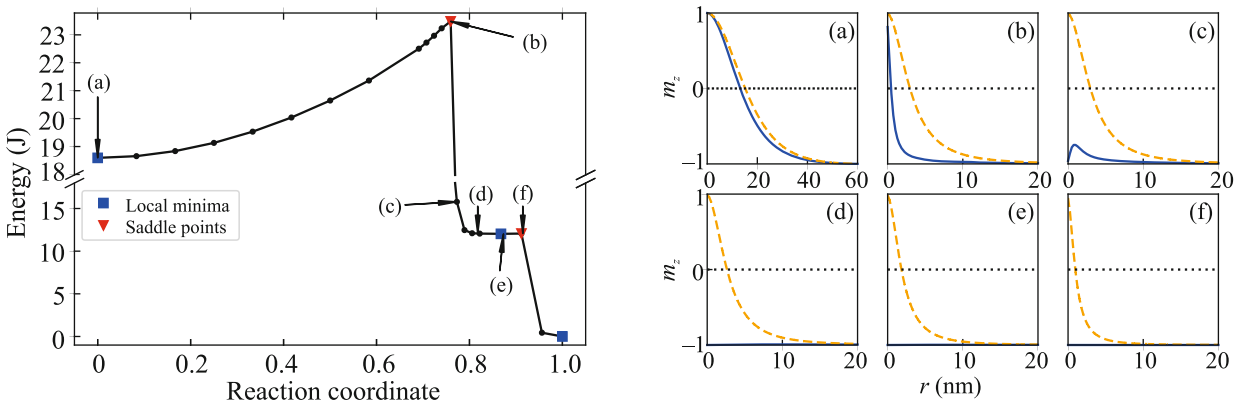

Fig. 4. (Color online) Minimum energy path between the state of bound skyrmions in the synthetic antiferromagnet layers and a homogeneous state without skyrmions for $H_{ext} = 0$. The path involves an intermediate minimum corresponding to the state with one skyrmion in the upper layer. Local minima and saddle points are shown as squares and triangles, respectively. Right panels represent the magnetic profiles $m_z(r)$ along the path at the points indicated in the plot shown in the left panel. The blue solid line corresponds to the skyrmion in the upper layer.

in the continuous σ model equal to $4\pi qJ$, where q is the topological charge of the magnetic structure. After passing the second saddle point, the system transforms to a homogeneous state. The barrier for the nucleation of a one-skyrmion magnetic configuration turns out to be slightly higher than that for the formation of a bound skyrmion pair from this state.

In the SAFM exposed to the magnetic field, the MEP has a similar form, but the activation barriers increase, as do the sizes of the skyrmions. This is primarily due to a decrease in the energy in the initial equilibrium state, whereas the energy of the system at the saddle point changes much less. The activation energy for the collapse of the one-skyrmion state also increases, being about $0.25J$ at $\mu_0 H_{ext} = 30$ mT. The activation energy for the decay of the two-skyrmion state in this field is already as high as $6J$.

To compare the activation energy of a skyrmion pair in a SAFM and a thin FM film, we calculate the MEP for the collapse of a single skyrmion. The parameters are chosen the same as for the SAFM films, except for the applied magnetic field $\mu_0 H_{ext} =$ 25 mT chosen such that the sizes of the skyrmion states in the FM film and in the SAFM at zero field coincide. The general picture of the MEP and the mechanism of collapse are similar to those reported in [18, 26]. The calculated activation energy of the collapse, $\Delta E = 3.44J$, is significantly lower than the corresponding barrier in the SAFM. This agrees with the experimentally confirmed stability of skyrmion states in the SAFM [14].

Finally, let us compare the activation energy for the decay of the skyrmion state in the SAFM with the estimates obtained in [14], where it was assumed that the size of the skyrmions during annihilation decreases in both layers synchronously, and the contributions to the energy of the system were calculated as functions of the radius of skyrmions. For this purpose, within the continuous model, an ansatz was used for the shape of the skyrmion magnetic profile [27], including its radius R as a parameter, and the contributions from different interactions to the energy were calculated analytically [8]. Calculations have shown that the dependence of all contributions on the radius for relatively small skyrmions in SAFM layers can be approximated by linear functions. Although the continuous model obviously cannot give a good description on scales of several lattice constants, extrapolation of the energy for $R \to 0$ was used to estimate the activation energy. The value obtained in this way, which formally corresponds to zero-radius skyrmions, was taken as the activation energy required for the transition to a spatially homogeneous state. Then the activation energy for the collapse was obtained by subtracting the energy of the equilibrium state of a pair of skyrmions from this value, and for the chosen parameters, it equals $5.66J$.

This value is 16% larger than that found in the construction of the MEP and significantly overestimates the stability of the skyrmion pair at room temperature. For an accurate estimate of the lifetime, it is necessary to calculate the pre-exponential factor in Eq. (3), which is taken equal to 10^9 in [14] for all structures under study. In the absence of the long-range dipole interaction, which is suppressed in the SAFM, such a calculation can be carried out within the harmonic theory of the transient state [28].

4. CONCLISIONS

The stability of topological magnetic structures with respect to thermal fluctuations is the key requirement for using them as magnetic memory bits. The lifetime of magnetic states can be considered as a

quantitative measure of stability. The study of the MEP corresponding to the annihilation of skyrmions in the SAFM allows one to describe the mechanism of collapse and determine the activation energy of such a process. This value, according to (3), provides the main contribution to the lifetime.

A rigorous calculation has demonstrated that the energy barrier along the found MEP is 16% lower than the estimates obtained in [14] under the assumption of a simultaneous decrease in the radius of skyrmions in both layers up to their complete decay. Taking into account that the activation energy is equal to approximately $35k_BT$ at room temperature, this gives a decrease in the lifetime of the structure by about a factor of 270 as compared to the results of [14], although even in this case, the structures can be stable for quite a long time. To accurately determine this time, it is necessary to know all the parameters in the Arrhenius law (3). Knowing the morphology of the energy surface near local minima and the saddle point, one can accurately calculate the pre-exponential factor in Eq. (3). Its value can change significantly with an increase in the number of degrees of freedom that determine the dimension of the energy surface [29]. This issue will be studied elsewhere.

FUNDING

This work was supported by the Russian Science Foundation (project no. 22-22-00632, https://rscf.ru/project/22-22-00632/).

CONFLICT OF INTEREST

The authors declare that they have no conflicts of interest.

REFERENCES

1. A. A. Belavin and A. M. Polyakov, JETP Lett. **22**, 245 (1975).
2. R. Wiesendanger, Nat. Rev. Mater. **1**, 16044 (2016).
3. A. Fert, N. Reyren, and V. Cros, Nat. Rev. Mater. **2**, 17031 (2017).
4. K. M. Song, J. S. Jeong, B. Pan, X. Zhang, J. Xia, S. Cha, T. E. Park, K. Kim, S. Finizio, J. Raabe, J. Chang, Y. Zhou, W. Zhao, W. Kang, H. Ju, and S. Woo, Nat. Electron. **3**, 148 (2020).
5. K. Everschor-Sitte, J. Masell, R. M. Reeve, and M. Kläui, J. Appl. Phys. **124**, 240901 (2018).
6. K. Litzius, I. Lemesh, B. Krüger, et al., Nat. Phys. **13**, 170 (2017).
7. L. Smejkal, Y. Mokrousov, B. Yan, and A. H. MacDonald, Nat. Phys. **14**, 242 (2018).
8. F. Büttner, I. Lemesh, and G. S. D. Beach, Sci. Rep. **8**, 4464 (2018).
9. S. K. Kim, G. S. D. Beach, K. J. Lee, T. Ono, T. Rasing, and H. Yang, Nat. Mater. **21**, 24 (2022).
10. S. Woo, K. M. Song, X. Zhang, et al., Nat. Commun. **9**, 959 (2018).
11. L. Caretta, M. Mann, F. Büttner, K. Ueda, B. Pfau, C. M. Günther, P. Hessing, A. Churikova, C. Klose, M. Schneider, and D. Engel, Nat. Nanotechnol. **13**, 1154 (2018).
12. M. N. Potkina, I. S. Lobanov, H. Jónsson, and V. M. Uzdin, J. Appl. Phys. **127**, 213906 (2020).
13. R. A. Duine, K. J. Lee, S. S. P. Parkin, and V. D. Stiles, Nat. Phys. **14**, 217 (2018).
14. W. Legrand, D. Maccariello, F. Ajejas, S. Collin, A. Vecchiola, K. Bouzehouane, N. Reyren, V. Cros, and A. Fert, Nat. Mater. **19**, 34 (2020).
15. R. Chen, Y. Gao, X. Zhang, R. Zhang, S. Yin, X. Chen, X. Zhou, Y. Zhou, J. Xia, Y. Zhou, S. Wang, F. Pan, Y. Zhang, and C. Song, Nano Lett. **20**, 3299 (2020).
16. T. Ma, A. K. Sharma, R. Saha, A. K. Srivastava, P. Werner, P. Vir, V. Kumar, C. Felser, and S. S. P. Parkin, Adv. Mater. **320**, 2002043 (2020).
17. W. T. Coffey, D. A. Garanin, and D. J. McCarthy, Adv. Chem. Phys. **117**, 483 (2001).
18. I. S. Lobanov, M. N. Potkina, and V. M. Uzdin, JETP Lett. **113**, 801 (2021).
19. W. Legrand, N. Ronceray, N. Reyren, D. Maccariello, V. Cros, and A. Fert, Phys. Rev. Appl. **10**, 064042 (2018).
20. J. Unguris, R. J. Celotta, and D. T. Pierce, Phys. Rev. Lett. **67**, 140 (1991).
21. P. F. Bessarab, V. M. Uzdin, and H. Jónsson, Phys. Rev. B **85**, 184409 (2012).
22. P. F. Bessarab, V. M. Uzdin, and H. Jónsson, Comput. Phys. Commun. **196**, 335 (2015).
23. I. S. Lobanov, V. M. Uzdin, and H. Jónsson, Phys. Rev. B **94**, 174418 (2016).
24. I. S. Lobanov and V. M. Uzdin, Comput. Phys. Commun. **269**, 108136 (2021).
25. I. S. Lobanov, M. N. Potkina, V. M. Uzdin, and H. Jónsson, Nanosyst.: Phys. Chem. Math. **8**, 586 (2017).
26. P. F. Bessarab, G. P. Müller, I. S. Lobanov, F. N. Rybakov, N. S. Kiselev, H. Jónsson, V. M. Uzdin, S. Blügel, L. Bergqvist, and A. Delin, Sci. Rep. **8**, 3433 (2018).
27. N. Romming, A. Kubetzka, C. Hanneken, K. von Bergmann, and R. Wiesendanger, Phys. Rev. Lett. **114**, 177203 (2015).
28. M. N. Potkina, I. S. Lobanov, O. A. Tretiakov, H. Jónsson, and V. M. Uzdin, Phys. Rev. B **102**, 134430 (2020).
29. M. N. Potkina, I. S. Lobanov, H. Jónsson, and V. M. Uzdin, J. Magn. Magn. Mater. **549**, 168974 (2022).

Translated by K. Kugel